

Molecular Theory of Nucleation from Dilute Phases: Formulation and Application to Lennard-Jones Vapor

Ravi Kumar Reddy Addula¹ and Sudeep N. Punnathanam^{1*}

Department of Chemical Engineering, Indian Institute of Science, Bengaluru 560012, India

(Received 14 October 2020; revised 8 March 2021; accepted 9 March 2021; published 8 April 2021)

In this Letter, we present a molecular theory of nucleation from dilute phases such as vapors or dilute solutions. The theory can model the nonclassical two-step crystal nucleation seen in many systems. When applied to study and analyze the crystal nucleation pathways from Lennard-Jones vapor, we find that prior explanations of the two-step mechanism based on lower barrier height for liquid nuclei is incomplete. The analysis from the molecular theory reveal that a complete explanation would also require consideration of anisotropy in the diffusion constants for growth of liquid droplets *vis-à-vis* the crystal nuclei.

DOI: 10.1103/PhysRevLett.126.146001

Although the phenomenon of nucleation has been widely studied, there still exist gaps in our understanding of its mechanism. Toward this end, we present a new theory for nucleation from dilute phases called “molecular theory of nucleation.” A dilute phase is defined as the one where the concentration of the component that forms the nucleus is low, such as vapors and dilute solutions. The basic statistical mechanics of this theory is similar to the one developed in Senger *et al.* [1] and Auer and Frenkel [2]. We then use the molecular theory to revisit the problem of crystal nucleation from a Lennard-Jones vapor phase [3,4] and predict the nucleation rates for a range of values of supersaturation. We show that the molecular theory can also model the nonclassical two-step mechanism seen in these systems.

Based on previous observations [3,4], we characterize the nuclei formed during crystal nucleation by two variables, namely, (i) the number of particles that form a connected cluster n and (ii) the number of particles within that cluster that form the largest crystalline nucleus m . Obviously, by construction, $m \leq n$. Now consider a population of such nuclei within a metastable fluid consisting of N particles in volume V at temperature T . Defining f as the number density of such nuclei, the kinetics of nucleation can be modeled by the following Fokker-Planck type equations [5]:

$$\frac{\partial f}{\partial t} = -\nabla \cdot \mathbf{J}, \quad (1)$$

$$\mathbf{J} = -D_m f^{(\text{eq})} \frac{\partial f}{\partial m} \frac{f}{f^{(\text{eq})}} \hat{\mathbf{e}}_m - D_n f^{(\text{eq})} \frac{\partial f}{\partial n} \frac{f}{f^{(\text{eq})}} \hat{\mathbf{e}}_n, \quad (2)$$

where \mathbf{J} is the nucleation flux in the (m, n) space, D_m and D_n are the diffusivities in m and n coordinates, respectively, and $f^{(\text{eq})}$ is the equilibrium number density of the nuclei in the metastable vapor. In the above equations, it is assumed that m and n vary continuously and one can differentiate f

with respect to these variables. The changes in m and n during nucleation are expected to be uncorrelated, and hence the diffusion tensor is assumed to be diagonal. At steady state, the above equations reduce to the following second-order partial differential equation:

$$\frac{\partial}{\partial m} D_m f^{(\text{eq})} \frac{\partial f}{\partial m} \frac{f}{f^{(\text{eq})}} + \frac{\partial}{\partial n} D_n f^{(\text{eq})} \frac{\partial f}{\partial n} \frac{f}{f^{(\text{eq})}} = 0. \quad (3)$$

The boundary conditions for Eq. (3) are shown in Fig. 1. The nucleation rate j is obtained by integrating \mathbf{J} over the boundaries \mathcal{C} and \mathcal{D} , i.e.,

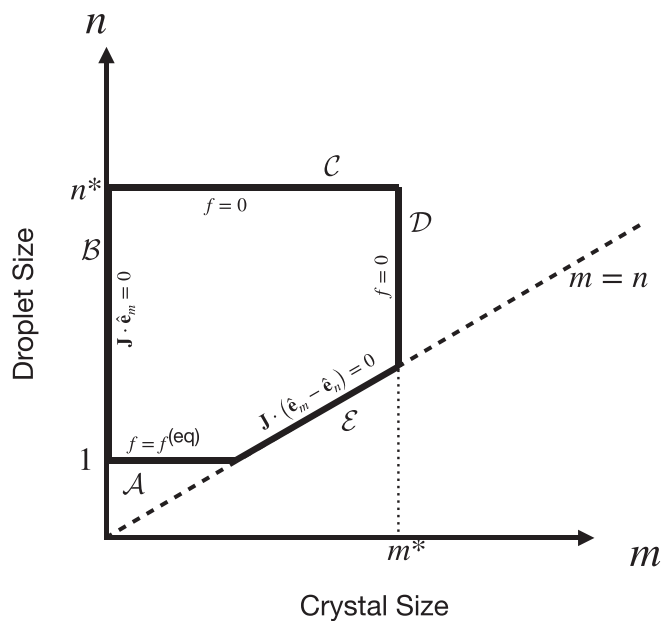


FIG. 1. Boundary conditions for solving Eq. (3). The letters \mathcal{A} , \mathcal{B} , \mathcal{C} , \mathcal{D} , and \mathcal{E} represent the boundaries of the domain for integration.

$$j = j_n + j_m = \int_C \mathbf{J} \cdot \hat{\mathbf{e}}_n ds + \int_D \mathbf{J} \cdot \hat{\mathbf{e}}_m ds,$$

where ds is the differential arc length. The equilibrium distribution $f^{(\text{eq})}$ is related to the work of formation of the nuclei $W_{m,n}$ as follows: $f^{(\text{eq})} = \rho_v \exp(-\beta W_{m,n})$, where ρ_v is the number density of the molecules in the vapor phase. It is possible to write an exact expression for $W_{m,n}$ using statistical mechanics as follows (see Supplemental Material [6] for the derivation):

$$\beta W_{m,n} = -(n-1) \ln \rho_v \Lambda^3 + \ln n! - n\beta\mu^{\text{ex}} + \beta(F_n^* + \Delta F_n^{\text{ins}} + \Delta F_{m|n}), \quad (4)$$

$$\beta F_n^* = -\ln \left[\frac{1}{\Lambda^{3(n-1)}} \int e^{-\beta U_n} \xi(\mathbf{r}^n) d\mathbf{r}^{n-1} \right], \quad (5)$$

$$\beta \Delta F_n^{\text{ins}} = -\ln \langle e^{-\beta U_\sigma} \zeta_n(\mathbf{r}^N) \rangle, \quad (6)$$

$$\beta \Delta F_{m|n} = -\ln \langle \omega_m(\mathbf{r}^n) \rangle, \quad (7)$$

where μ^{ex} is the excess chemical potential in the metastable phase, U_n is the energy of the n molecule cluster, and U_σ is the energy of interaction between the cluster and the surrounding metastable phase. The physical interpretation of the various terms on the rhs of Eq. (4) are as follows. F_n^* is the free energy of an n particle cluster with one of the particles kept fixed. ΔF_n^{ins} is the free-energy change upon insertion of this n particle cluster into the metastable phase, and $\Delta F_{m|n}$ is the free-energy of formation of an m particle crystalline nucleus within the n particle cluster. The functions ξ , ω , and ζ are defined as follows:

$$\xi(\mathbf{r}^n) = \begin{cases} 1 & \text{if the } n \text{ particles form a connected cluster} \\ 0 & \text{otherwise} \end{cases},$$

$$\omega_m(\mathbf{r}^n) = \begin{cases} 1 & \text{if } m \text{ particles out of } n \text{ form the largest crystalline nucleus} \\ 0 & \text{otherwise} \end{cases},$$

$$\zeta_n(\mathbf{r}^N) = \begin{cases} 0 & \text{if any of } N - n \text{ particles belong to the cluster} \\ 1 & \text{otherwise} \end{cases}.$$

These constraints ensure that only the relevant configurations are counted while evaluating the partition function.

If concentration of the component that forms the nucleus is very low (such as vapors or solutions of sparingly soluble solutes), then the terms ΔF_n^{ins} and $\Delta F_{m|n}$ can be assumed to be independent of the supersaturation. Hence, the dependence of $W_{m,n}$ on supersaturation is contained in the first and third terms of Eq. (4), which can be evaluated either from equation of state for vapor phases or from activity coefficients for solutions. Equation (3) along with Eqs. (4)–(7) constitute the main result of the molecular theory of nucleation for dilute phases.

To demonstrate the application of the molecular theory, we revisit a previous study of crystal nucleation from a dilute vapor by van Meel *et al.* [4]. The intermolecular interactions are modeled by Lennard-Jones potential that has been truncated and shifted at a cutoff distance, $r_c = 2.5\sigma$. The phase diagram for this system is given in the Supplemental Material [6]. The crystal nucleation is studied at the reduced temperature $T^* = 0.45$, which is below the triple point. At this temperature, the coexistence pressure between the vapor and the solid is $P_{v,s}^{*,\text{sat}} = 2.28 \times 10^{-5}$ and that between the vapor and the liquid is $P_{v,l}^{*,\text{sat}} = 4.28 \times 10^{-5}$ [4], indicating that the vapor-liquid equilibrium is metastable. Since the density of the vapor phase is very low, it can be approximated as an ideal gas and the values of μ^{ex} and ΔF_n^{ins} can be set to zero. As a result, Eq. (4) simplifies to

$$\beta W_{m,n} = -(n-1) \ln(\rho_v \Lambda^3) + \ln n! + \beta(F_n^* + \Delta F_{m|n}). \quad (8)$$

The criteria used to identify the liquid cluster as well as the crystal nucleus within the liquid cluster are the same as the one used in Ref. [4]. A snapshot of the crystal nucleus within the liquid cluster is given in the Supplemental Material [6]. The quantity F_n^* is computed using a variant of the Einstein-molecule method [7] and $\Delta F_{m|n}$ is computed from umbrella sampling simulations of an n molecule cluster (for details, see the Supplemental Material [6]). The values of $\Delta F_{m|n}$ are fitted to a model based on a feed forward neural network (for details, see the Supplemental Material [6]) due to high degree of nonlinearity. The free-energy landscape for droplet nucleation $W_{m=0|n}$ is fitted to the following equation:

$$\beta W_{m=0|n} = -(n-1) \ln(\rho_v \Lambda^3) + \ln n! + a_1(n-1) + a_2(n-1)^{2/3} + a_3(n-1)^{1/3} + a_4(n-1)^{1/6}. \quad (9)$$

The third and fourth terms on the rhs correspond to volume and surface dependence, while the fifth and the sixth term are additional corrections determined empirically. In the discussion that follows, we discuss the nucleation mechanism at two pressures; namely, $P^* = 2 \times 10^{-4}$ and $P^* = 1.03 \times 10^{-4}$. The motivation for the choice of these pressures is given in the Supplemental Material [6].

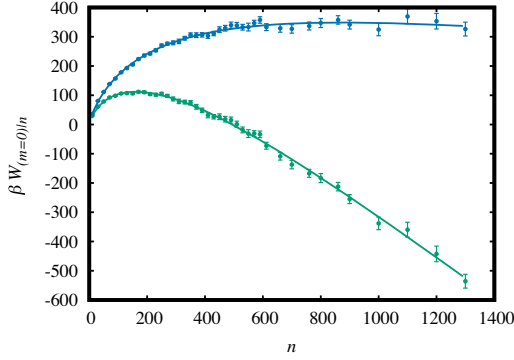


FIG. 2. Variation of $W_{m=0|n}$ vs n at $T^* = 0.45$. The symbols are values computed from simulations and the line is the prediction using Eq. (9). The blue color data are at $P^* = 1.03 \times 10^{-4}$ and the green color data are at $P^* = 2.0 \times 10^{-4}$. The size of error bars correspond to a confidence interval of 90%.

The computed values of $W_{m=0|n}$ and the fit from Eq. (9) are shown in Fig. 2. As expected, the values of $W_{m=0|n}$ show a maximum, which is the location of the critical liquid nucleus. The estimates of the size of the critical nuclei from these plots are in agreement with the results reported in Ref. [4]. Figure 3 shows a contour plot of $W_{m,n}$ at these two pressures. At $P^* = 2 \times 10^{-4}$, the free-energy landscape shows only one maximum at $n = 160$ and $m = 0$. At lower

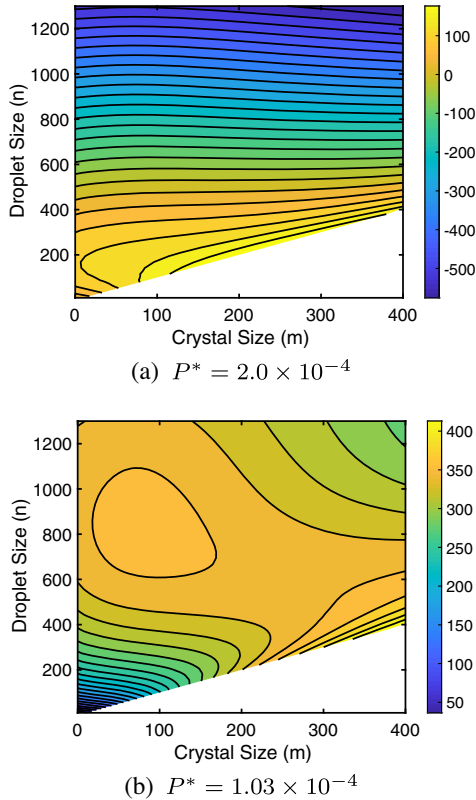


FIG. 3. Contour plots of the free-energy landscape $W_{m,n}$ for vapor to crystal nucleation at (a) $P^* = 2 \times 10^{-4}$ and (b) $P^* = 1.03 \times 10^{-4}$.

values of n , $W_{m,n}$ increases monotonically with m . At around $n = 550$, the values of $W_{m,n}$ start to show a maximum for given droplet size, i.e., at constant n . These maxima, which represent the barrier to crystal nucleation within the droplets, are located around $m = 80$ and are nearly insensitive to the value of n . The occurrence of these maxima, however, does not result in appearance of a saddle point in the free-energy landscape. The minimum free-energy path is given by the line $m = 0$ with a single maximum. As we shall see later, the two-step mechanism is a result of the anisotropy in the diffusion constants. If the pressure of the vapor phase is lowered, one begins to see a saddle point in the free-energy surface. In Fig. 3(b), we show the free-energy landscape at $P^* = 1.03 \times 10^{-4}$. At this pressure there exist two critical nuclei: (i) at $n = 880$ and $m = 0$ and (ii) at $n = 600$ and $m = 250$. Both these critical nuclei have nearly the same free-energy barrier of $\beta W_{m,n} \approx 350$. Again, as we shall see later, the diffusion anisotropy plays a decisive role in the selection of the nucleation pathway.

To compute the nucleation pathway and the rate, we solved Eq. (3) numerically using the finite volume method. The boundaries for integration were set to $n^* = 1300$ and $m^* = 400$. The values of D_m and D_n were computed from swarms of molecular dynamics trajectories at the top of the free-energy barriers. We assume that D_m and D_n are proportional to $m^{2/3}$ and $n^{2/3}$, respectively; i.e., they are proportional to the surface area of the nuclei. At $P^* = 2 \times 10^{-4}$, the nucleation rate (in reduced units) was computed to be 1.79×10^{-58} . This corresponds to a rate of $2.4 \times 10^{-18} \text{ m}^{-3} \text{ s}^{-1}$ for argon vapor at 64 K and 10^4 Pa . The solution of Eq. (3) also enables us to determine the nucleation pathways in these systems. In Fig. 4(a), we show 100 streamlines depicting the flux of nucleation on top of the free-energy landscape. The starting points of each streamline were chosen from an equilibrium distribution of precritical nuclei in the subcooled vapor. The computed nucleation pathways clearly deviate from the minimum free-energy path and show a two-step mechanism for vapor to crystal nucleation. The first nucleation step is a conventional barrier crossing step leading to formation of liquid droplets. The crystallinity of most of the critical droplets are negligible but some can contain crystal nuclei with value of $m = 20$. The existence of the second nucleation step, even though the free energy is continuously decreasing, lies in the anisotropy in the diffusion constants. The ratio $D_m/D_n \approx 7 \times 10^3$ because the low density of the vapor phase causes the rate of droplet growth to be very slow. In the absence of diffusion anisotropy, the nucleation pathway follows the minimum free-energy path, as can be seen in Fig. 4(b), and the ratio $j_m/j_n = 3.4 \times 10^{-21}$, indicating hardly any crystal nucleation events. At $P^* = 1.03 \times 10^{-4}$, we see another consequence of the diffusion anisotropy. The diffusion anisotropy is $D_m/D_n \approx 10^4$ and the nucleation rate (in reduced units) is 1.78×10^{-158} . This

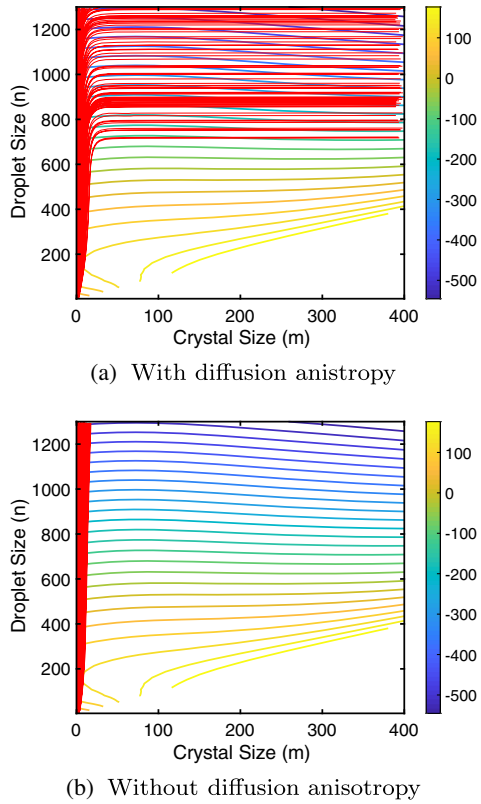


FIG. 4. Streamlines (red lines) showing flux of vapor to crystal nucleation on top of the free-energy landscape at $P^* = 2.0 \times 10^{-4}$ (a) with and (b) without diffusion anisotropy.

corresponds to a rate of $2.4 \times 10^{-118} \text{ m}^{-3} \text{ s}^{-1}$ for argon vapor at 64 K and $5 \times 10^3 \text{ Pa}$. As a result, even though the free-energy barriers for the two critical nuclei are nearly equal, almost all of the nucleation pathways pass through the saddle point corresponding to the crystal nucleus [see Fig. 5(a)]. This is reflected in the value of the ratio $j_m/j_n = 4.9 \times 10^9$. The initial fluctuation, however, consists of formation of liquid droplets, but these droplets are still precritical when the formation of crystal nuclei occurs inside them. If we discount the diffusion anisotropy, then we observe two distinct nucleation pathways [see Fig. 5(b)]: one where hardly any crystal nucleation occurs in droplets up to size $n = 1300$, and the other where nucleation of crystal from vapor occurs in a single step. In the second pathway, the initial fluctuation contains a significant amount of crystalline structure. The computed value of the ratio $j_m/j_n = 14.6$ reflecting that both the nucleation pathways are competitive. The low value of the nucleation rate indicates that at these temperatures, which lie just below the triple point, the nucleation mechanism for realistic rates would always involve formation of liquid droplets. Indeed, experimental studies of nucleation from argon vapor at temperatures below the triple point show the formation of liquid droplets [8]. It is also one of the strengths of the molecular theory approach that one is able

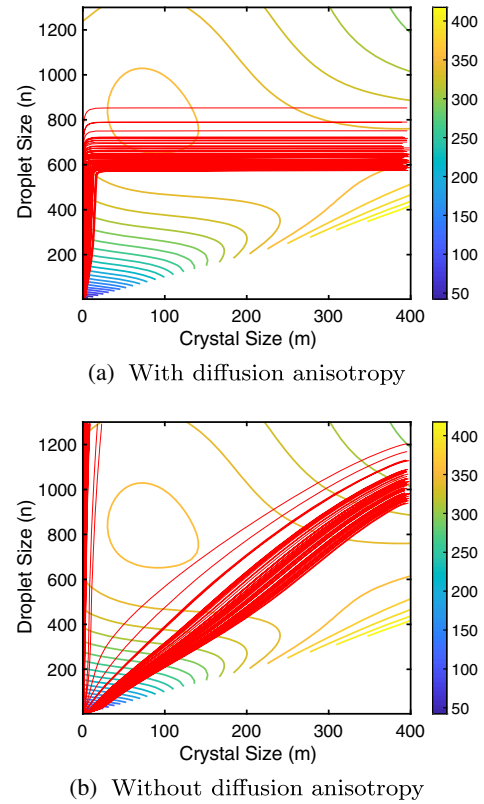


FIG. 5. Streamlines (red lines) showing flux of vapor to crystal nucleation on top of the free-energy landscape at $P^* = 1.03 \times 10^{-4}$ (a) with and (b) without diffusion anisotropy.

to compute such low rates of nucleation, which would otherwise require much longer simulations using other methods [3,4].

While the deviation of the transition paths from the minimum free-energy path in activated systems due to diffusion anisotropies has been known for some time [9] and also studied within the context of crystal nucleation [10], its role towards changing the mechanism from one-step to two-step has not been shown before. Previous studies have either ignored the role of diffusion anisotropy [11] or given it a cursory attention [12], and hence their explanations of the two-step mechanism were incomplete.

Finally, in Fig. 6, we plot the nucleation rate for a range of supersaturations as predicted by the molecular theory. In this calculation, D_n is assumed to be directly proportional to ρ_v , while D_m is assumed to be independent of ρ_v . The overall computational effort needed to calculate this curve is similar to that needed in simulation [3,4] of nucleation at a single value of supersaturation. In the inset, we compare the predictions of the molecular theory with nucleation rate for liquid drops using the classical nucleation theory (since the initial fluctuation is that of a liquid cluster). The nucleation rate from classical nucleation theory j_{CNT} is given by

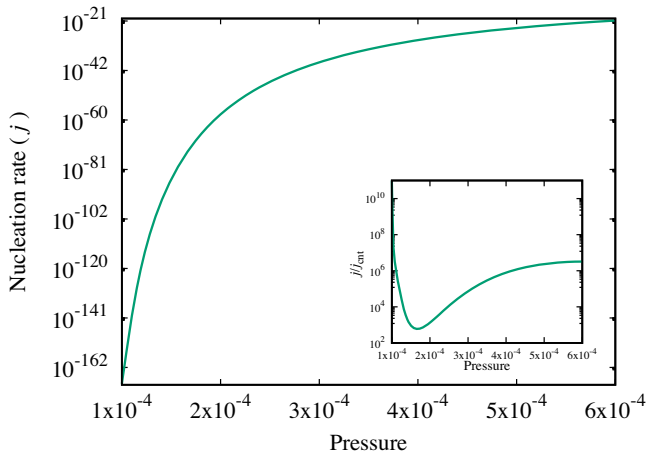


FIG. 6. Nucleation rate as predicted by the molecular theory at various pressures. Inset: ratio of the nucleation rate with that predicted by classical nucleation theory.

$$j_{\text{CNT}} = D_n \rho_v \sqrt{\frac{\Delta\mu}{6\pi k_B T n^*}} \exp\left(-\frac{\Delta G^*}{k_B T}\right),$$

$$\Delta\mu = k_B T \ln(P/P_{v,i}^{\text{sat}}), \quad R = \frac{2\gamma}{|\rho_l \Delta\mu|},$$

$$n^* = \frac{4}{3} \pi R^3 \rho_l, \quad \Delta G^* = \frac{16\pi\gamma^3}{3|\rho_l \Delta\mu|^2},$$

where γ is the surface tension and ρ_l is the density of the liquid phase. The values of γ and ρ_l were taken from Ref. [4] and are equal to 1.07 and 0.905, respectively. The nucleation rate predicted by the molecular theory is higher than j_{CNT} . The ratio j/j_{CNT} shows a minimum that roughly corresponds to pressures where one starts to see crystal nucleation in precritical liquid droplets.

The usefulness of the molecular theory extends beyond describing crystal nucleation from vapor phases. Simulations of crystal nucleation from solutions are plagued by many technical challenges [13]. Unlike nucleation from a melt, the mechanism of nucleation from solutions is dominated by slow diffusion of solute molecules from the bulk to the crystal-solution interface. There is also a challenge of maintaining constant supersaturation within the bulk as the nuclei in the solution grow [14]. Through the use of Eq. (4), these difficulties encountered in the simulations can be overcome.

The authors thank Professor David Corti, Purdue University for a critical reading of this Letter. This work is funded Department of Science and Technology, Government of India (Grant No. CRG/2019/003681).

*sudeep@iisc.ac.in

- [1] B. Senger, P. Schaaf, D. S. Corti, R. Bowles, J. C. Voegel, and H. Reiss, *J. Chem. Phys.* **110**, 6421 (1999).
- [2] S. Auer and D. Frenkel, *J. Chem. Phys.* **120**, 3015 (2004).
- [3] B. Chen, H. Kim, S. J. Keasler, and R. B. Nellas, *J. Phys. Chem. B* **112**, 4067 (2008).
- [4] J. A. van Meel, A. J. Page, R. P. Sear, and D. Frenkel, *J. Chem. Phys.* **129**, 204505 (2008).
- [5] D. Reguera, J. M. Rubi, and A. Perez-Madrid, *Physica (Amsterdam)* **259A**, 10 (1998).
- [6] See Supplemental Material at <http://link.aps.org/supplemental/10.1103/PhysRevLett.126.146001> for derivation of work of formation $W_{m,n}$, Choice of pressures to study nucleation, Details of neural network fitting for $\Delta F_{m|n}$, Einstein Molecule method for computing F_n^* , Phase diagram and Snapshot of the critical nucleus.
- [7] C. Vega and E. G. Noya, *J. Chem. Phys.* **127**, 154113 (2007).
- [8] A. Fladerer and R. Strey, *J. Chem. Phys.* **124**, 164710 (2006); K. Iland, J. Wolk, R. Strey, and D. Kashchiev, *J. Chem. Phys.* **127**, 154506 (2007).
- [9] A. Berezhkovskii and A. Szabo, *J. Chem. Phys.* **122**, 014503 (2005).
- [10] R. P. Sear, *J. Chem. Phys.* **128**, 214513 (2008); B. Peters, *J. Chem. Phys.* **131**, 244103 (2009).
- [11] P. R. ten Wolde and D. Frenkel, *Science* **277**, 1975 (1997).
- [12] D. James, S. Beairsto, C. Hartt, O. Zavalov, I. Saika-Voivod, R. K. Bowles, and P. H. Poole, *J. Chem. Phys.* **150**, 074501 (2019).
- [13] M. Salvalaglio, C. Perego, F. Giberti, M. Mazzotti, and M. Parrinello, *Proc. Natl. Acad. Sci. U.S.A.* **112**, E6 (2015); T. Karmakar, P. M. Piaggi, and M. Parrinello, *J. Chem. Theory Comput.* **15**, 6923 (2019); C. Liu, G. P. F. Wood, and E. E. Santiso, *Mol. Phys.* **116**, 2998 (2018).
- [14] V. Agarwal and B. Peters, *Solute Precipitate Nucleation: A Review of Theory and Simulation Advances*, edited by S. A. Rice and A. R. Dinner, *Advances in Chemical Physics* Vol. 155 (John Wiley & Sons Inc., New York, 2014), pp. 97–159, <https://doi.org/10.1002/9781118755815.ch03>.